# Adsorption of hydrophobic polyelectrolytes as studied by *in situ* high energy X-Ray reflectivity

Damien Baigl,[1,2,*] Marie-Alice Guedeau-Boudeville,[1] Raymond Ober,[1] François Rieutord,[3] Michele Sferrazza,[4] Olivier Théodoly,[5] Thomas A. Waigh,[6] and Claudine E. Williams[1,†]

[1] *Laboratoire de Physique des Fluides Organisés, CNRS UMR 7125, Collège de France, Paris, France*
[2] *Dept of physics, Graduate school of science, Kyoto University, Kyoto 606-8502, Japan*
[3] *DRFMC-SI3M, CEA-Grenoble and ESRF BM32 beamline, Grenoble, France*
[4] *Département de Physique, Université Libre de Bruxelles, Bruxelles, Belgium*
[5] *Complex Fluids Laboratory, CNRS/Rhodia UMR 166, Cranbury, NJ 08512, USA*
[6] *Department of Physics and Astronomy, University of Leeds, Leeds, LS2 9JT, UK*

(Dated: February 2, 2008)

A series of well-defined hydrophilic and hydrophobic polyelectrolytes of various chain lengths $N$ and effective charge fractions $f_{eff}$ have been adsorbed onto oppositely charged solid surfaces immersed in aqueous solutions. *In situ* high energy X-ray reflectivity has provided the thickness $h$, the electron density and the roughness of the adsorbed layer in its aqueous environment. In the case of hydrophobic polyelectrolytes, we have found $h \propto N^0 f_{eff}^{-2/3}$, in agreement with a pearl-necklace conformation for the chains induced by a Rayleigh-like instability.

PACS numbers: 68.08.-p, 68.55.-a, 82.35.Rs, 82.35.Lr

## I. INTRODUCTION

Polyelectrolytes are macromolecules containing ionizable groups which, in a polar solvent like water, dissociate into charges tied to the polymer backbone and counter-ions dispersed in the solution. They are called hydrophobic when water is a poor solvent for the backbone. As amphiphilic water-soluble macromolecules, hydrophobic polyelectrolytes are of great interest for industrial applications; in nature, many biological macromolecules, proteins for instance, have some intrinsic hydrophobicity. However, even if experiments [1, 2, 3], theories [4, 5, 6] and simulations [7, 8] are now all consistent with a pearl-necklace conformation for the single chain, the physics of hydrophobic polyelectrolytes is still far from being fully understood. Indeed, the role of counterions, the long-range electrostatic interactions, the short-range monomer-monomer interactions and solvent effects make simulations and theories difficult to achieve. On the experimental side, the combination of poor contrast in scattering experiments and fluctuations of concentration with a wide range of length scales (from a few nanometers for the pearl size up to a micron for the Debye length in pure water) make the interpretation of bulk properties in salt-free solutions rather delicate [9, 10]. Adsorbing chains onto solid surfaces is an interesting way to freeze the fluctuations of concentration and eventually those of conformation [11]. *In situ* characterization of the solid-liquid interface can then provide an insight into the properties of the chains trapped within the adsorbed layer. Beside techniques such as AFM [12] and *in situ* ellipsometry [13] which provide the local surface topography and the average adsorbed amount, respectively, X-ray reflectivity has the advantage of providing the electron density profile [14, 15]. So far, *in situ* X-ray reflectivity has been applied to only a few systems such as lamellar phases [16] or polyelectrolyte multilayers [17]. However, to our knowledge, it has never been used to characterize a polyelectrolyte monolayer in its aqueous environment at the solid-liquid interface.

In this paper we present an experimental study of model hydrophobic polyelectrolyte monolayers adsorbed onto oppositely charged or hydrophobic solid surfaces. Adsorbed layers were characterized *in situ*, *i.e.*, inside the aqueous solution at the solid-liquid interface, by the technique of X-ray reflectivity with high energy photons. In a previous study, we have used *in situ* ellipsometry to investigate the properties of hydrophobic polyelectrolyte monolayers adsorbed onto oppositely charged solid surfaces. It has allowed us to establish the conditions for which the pearl-necklace conformation of the chains persisted upon adsorption. This required the presence of added salt in order for the Debye length to be comparable to the pearl size. In this case, the thickness of the adsorbed layer is proportional to the pearl size [18]. For the present study, the adsorbed layer has been prepared with the same operating conditions (oppositely charged solid surface and presence of added salts) and we have measured the thickness of the adsorbed layer, its roughness and its electron density as a function of the chemical charge fraction and the length of the chains. In order to investigate the effect of the solvent quality, we have made a parallel study of the adsorption of a model hydrophilic polyelectrolyte. Finally, since hydrophobic polyelectrolytes are amphiphilic molecules [19], we present preliminary results for the adsorption onto neutral hydrophobic solid surfaces.

*baigl@chem.scphys.kyoto-u.ac.jp
†claudine.williams@college-de-france.fr

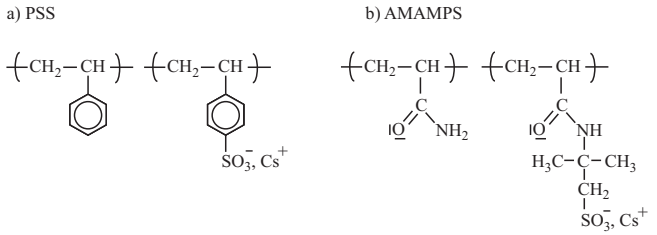


FIG. 1: Chemical structures of a) PSS, a model hydrophobic polyelectrolyte and b) AMAMPS, a model hydrophilic polyelectrolyte. Both are random copolymers.

## II. EXPERIMENTAL SECTION

Throughout this paper, the following notations will be used: $h$ for thickness, $\rho$ for electron density, $\sigma$ for roughness, Si for silicon, SiO2 for silica, SAM for Self-Assembled Monolayer, PCS for oppositely charged surface, HS for hydrophobic surface, PSS for the hydrophobic polyelectrolyte (poly(styrene-*co*-styrenesulfonate)) and AMAMPS (poly(acrylamide-*co*-acrylamidomethylpropanesulfonate)) for the hydrophilic polyelectrolyte.

### A. Materials

#### 1. Hydrophobic polyelectrolytes

As a model hydrophobic polyelectrolyte we have used poly(styrene-*co*-styrenesulfonate, cesium salt), abbreviated PSS (see figure 1a). This random copolymer is soluble in water when it contains more than 30% of styrenesulfonate monomers on average. Therefore, the resulting macromolecule is a water-soluble charged polymer having a very hydrophobic backbone of polystyrene and it can be considered as a model hydrophobic polyelectrolyte. A series of well-defined monodisperse PSS of various chain lengths $N$ and chemical charge fractions $f$, *i.e.*, molar percentage of styrenesulfonate per chain, have been synthesized and characterized according to a procedure described elsewhere [20]. Previous osmotic pressure and freezing point depression measurements have shown a strong reduction of the effective charge fraction $f_{eff}$ as a function of $f$. We have found that $f_{eff}$ obeys the following empirical renormalization law [1, 21]:

$$f_{eff}(\%) = 100\frac{f - f^*}{100 - f^*}\frac{a}{l_B} = \frac{f(\%) - 18}{82}36 \qquad (1)$$

where $f^*$ is the chemical charge fraction (18%) at which $f_{eff}$ equals 0, $a$ is the monomer size (0.25 nm) and $l_B$ is the Bjerrum length (0.71 nm in pure water at 25°C). The characteristics of PSS samples used in this study are summarized in Table I.

TABLE I: PSS samples of various chain lengths $N$, chemical charge fractions $f$ and effective charge fractions $f_{eff}$. $f_{eff}$ is estimated from $f$ using eq. 1

| $N$ | $f(\%)$ | $f_{eff}(\%)$ | $N$ | $f(\%)$ | $f_{eff}(\%)$ |
|---|---|---|---|---|---|
| 930 | 33 | 6.6 | 1320 | 36 | 7.9 |
| 930 | 41 | 10.1 | 1320 | 53 | 15.4 |
| 930 | 46 | 12.3 | 1320 | 71 | 23.3 |
| 930 | 62 | 19.3 | 1320 | 91 | 32.0 |
| 930 | 83 | 28.5 | 2520 | 37 | 8.3 |
| | | | 2520 | 54 | 15.8 |
| | | | 2520 | 89 | 31.2 |

#### 2. Hydrophilic polyelectrolytes

As a model hydrophilic polyelectrolyte we have used poly(acrylamide-*co*-acrylamidomethylpropanesulfonate, cesium salt), abbreviated AMAMPS (see figure 1b) because its polyacrylamide backbone is water soluble. Here the chemical charge fraction $f$ is the molar percentage of acrylamidomethylpropanesulfonate monomer per chain and it was measured by $^1$H NMR (Bruker Avance300 spectrometer) in deuterium oxide (Aldrich). AMAMPS's with $f$ ranging from 34% to 100% have been synthesized by radical copolymerization of acrylamide (Aldrich) and sodium 2-acrylamido-2-methyl-1-propanesulfonate, initiated by potassium persulfate and tetradimethylethylenediamine (Aldrich), in a 60/20 water-ethanol mixture according to a procedure inspired from [22] and fully described in [1].

#### 3. Surfaces

Two types of solid surfaces have been prepared, as pictured in figure 2: a) positively charged surface (PCS) and b) neutral hydrophobic surface (HS). For this purpose, self-assembled monolayers (SAM) have been grafted on the native silica layers covering silicon wafers (Siltronix, Archamps, France; diameter: 25.4 mm, thickness: 2 mm). First, each wafer is cleaned by a 45 minutes UV-$O_3$ treatment prior to 15 minutes exposure under an oxygen flow saturated with water. Right after this activation process, the wafer is immersed in 15 mL of a freshly prepared silane (Aminopropyltrimethoxysilane (a) or Phenyltrimethoxysilane (b), Aldrich) solution at 0.15 mol.L$^{-1}$ in anhydrous toluene (stored on molecular sieves) and left under gentle stirring during 15 minutes at ambient temperature. The wafer is then cautiously withdrawn to be rinsed thoroughly by pure anhydrous toluene followed by pure anhydrous chloroform. After rinsing, the wafer is dried with gaseous nitrogen (Air Liquide), left in a vacuum oven at 90°C for 12 minutes, rinsed again by pure anhydrous toluene and chloroform and dried under nitrogen flow. The wafer is finally stored under nitrogen in an airtight box. The silica

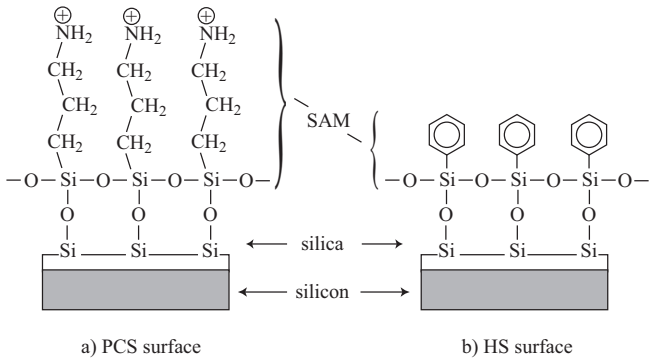


FIG. 2: Chemical structures of the planar solid surfaces. a) Positively charged surface (PCS) and b) hydrophobic surface (HS).

layer thickness $h_{SiO2}$ was measured by ellipsometry in air after activation and before silanation. The SAM thickness $h_{SAM}$ was measured by ellipsometry in air while its roughness $\sigma_{SAM}$ and density $\rho_{SAM}$ were measured by X-ray reflectivity in air at our laboratory. The topography was checked by atomic force microscopy. All these measurements are consistent with a dense self-assembled monolayer ($h_{SAM} = 1.1$ nm for PCS and 0.4 nm for HS, $\rho_{SAM} = 0.29$ e$^-$Å$^{-3}$, $\sigma_{SAM} = 0.5$ nm).

The adsorbed polyelectrolyte layers were prepared by spontaneous adsorption from aqueous solution of polymer at 0.01 mol.L$^{-1}$ and CsCl at 0.1 mol.L$^{-1}$. In these conditions it has been shown that the pearl-necklace conformation persists in the adsorbed state [18].

### B. *in situ* X-ray reflectivity

#### 1. Principles

The specular reflectivity $R$ is defined as the ratio of the reflected intensity to the intensity of the incident beam. An X-ray reflectivity experiment consists in measuring $R$ as a function of the incident angle $\theta$ or of the vertical momentum transfer $q$ ($q = 4\pi n/\lambda \sin\theta$ where $\lambda$ is the wavelength). The refractive index $n$ of matter for X rays is given by $n = 1 - \delta - i\beta$ where $\delta \approx \rho r_e \lambda^2/(2\pi)$, $\rho$ is the electron density and $r_e$ the classical electron radius, and $\beta = \mu\lambda/4\pi$ is related to the absorption coefficient $\mu$. For X-ray wavelengths, $\delta$ and $\beta$ are much less than 1. Neglecting absorption, an X-ray wave propagating in a medium 0 is totally reflected on a substrate 1 for $\theta < \theta_c$ ($q < q_c$ respectively), where the critical angle $\theta_c$ is given by

$$\theta_c \approx \sqrt{2(\delta_1 - \delta_0)} \tag{2}$$

For $\theta \geq \theta_c$, in the case of a sharp ideal interface, the reflectivity, called Fresnel reflectivity $R_F$, is approximately

$$R_F \approx \frac{\theta_c^4}{16\theta^4} = \frac{q_c^4}{16q^4} \tag{3}$$

For real surfaces, the reflectivity can be expressed as a function of the electron density profile [23]:

$$R = R_F \left| \int \frac{1}{\rho_0} \frac{d\rho}{dz} \exp(-iqz) dz \right|^2 \tag{4}$$

#### 2. Reflectivity experiment

Experimental conditions have been optimized regarding the strong absorption of X-ray radiation by water. The absorption coefficient $\alpha$, defined as the ratio of the transmitted intensity $I_t$ after travelling a distance $d$ to incident intensity $I_0$, can be expressed as $\alpha = I_t/I_0 = \exp(-\mu d)$. Since $\mu$ is a decreasing function of energy, high energy synchrotron radiation is necessary [24]. However, working angles decrease with energy since $\theta_c \propto E^{-1}$. Therefore, the longitudinal length $L$ of the corresponding footprint at $\theta_c$ (in the direction of beam propagation), $L = h/\sin\theta_c$, is an increasing function of $E$. Larger wafers are thus required at higher energy, implying an increase of $d$ and $\alpha$. The final choice of our experimental conditions was a compromise between these requirements as described below.

Experiments were performed on BM32 beamline of the European Synchrotron Radiation Facility (ESRF) in Grenoble (France) at a photon energy of 27 keV ($\lambda \approx 0.046$ nm) corresponding to a critical angle $\theta_c \approx 0.048°$ ($q_c \approx 0.23$ nm$^{-1}$) [25]. A point, low background scintillation detector has been used. The high precision beamline goniometer has been used in the range $0 \leq \theta \leq 0.76°$ ($0 \leq q \leq 3.6$ nm$^{-1}$). Working at such small angles requires perfectly planar surfaces. Hence, before each *in situ* reflectivity experiment, the planeity of the solid surface has been checked by measuring the width of the reflected beam. The incident beam has been limited by slits to a size of $l = 1$ mm (horizontal width) by $h = 20$ $\mu$m (vertical height). The corresponding footprint at $\theta_c$ had a longitudinal length $L \approx 23.9$ mm, which is slightly smaller than the wafer size (25.4 mm). The liquid cell, especially designed for these conditions, is illustrated in figure 3. Its diameter, 26 mm, is just above that of the solid surface. The watertight cylindrical structure is made of Kelev. This hydrophobic polymer material prevents chemical and ionic contamination. Windows have been made of Kapton, a non-absorbing material with negligible scattering. Since the solid surface is maintained by depression, it is important to use thick wafers (2 mm) to avoid deformation. The in/out vent system allows one to flush the cell with the surface kept immersed. Finally, with these conditions, the absorption coefficient was approximately $\alpha \approx 0.3$.

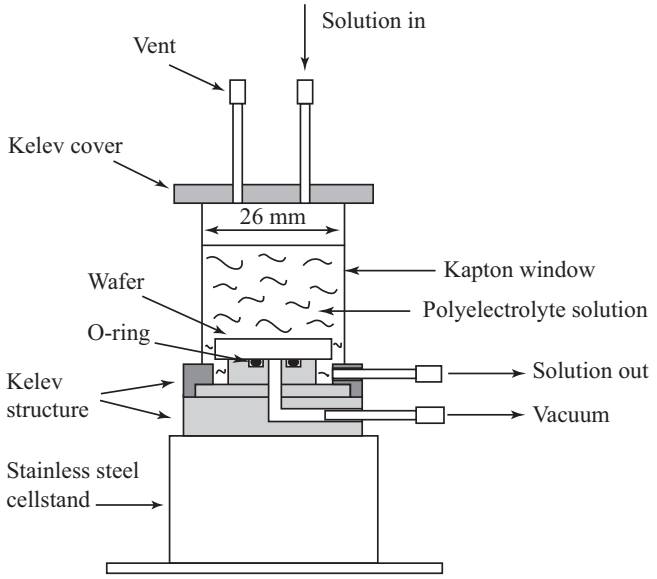


FIG. 3: Liquid cell for the reflectivity experiment.

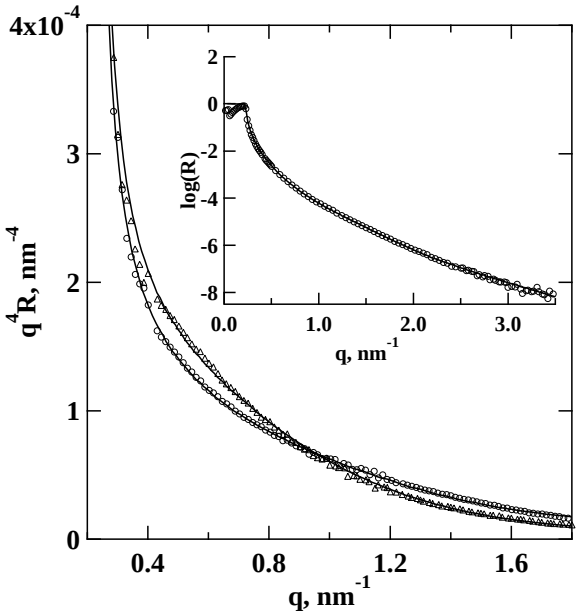


FIG. 4: $q^4R$ as a function of the vertical momentum transfer $q$ before (open triangles) and after the adsorption (open circles) of one PSS ($N = 2520$, $f = 37\%$). Inset: logarithm of reflectivity log(R) as a function of $q$ for the adsorbed PSS layer ($N = 2520$, $f = 37\%$). Solid lines result from fits using Parrat's algorithm (eq. 6-10).

The background for the reflectivity curve has been measured at an angle of $2\theta + 0.1°$ and substracted afterwards. It was checked that during the typical exposure time of about 15 minutes, no beam damage of the surface occurred.

## III. RESULTS AND DISCUSSION

### A. Experimental data

A typical reflectivity scan for the model hydrophobic polyelectrolyte (PSS) is presented in the inset of figure 4. The logarithm of reflectivity $\log(R)$ is plotted as a function of the vertical momentum transfer $q$ for an adsorbed PSS layer ($N = 2520$, $f = 37\%$) immersed in water. The critical edge at 0.23 nm$^{-1}$ is clearly visible. For $q < q_c$, $R$ is less than 1 for geometric reasons. For $q > q_c$, $R$ decreases steeply as a function of $q$. According to eq. 3, at a sharp silicon-water ideal interface, $R$ would be proportional to $q^{-4}$. In the main graph, $q^4R$ is plotted as a function of $q$ for a PCS surface before (open triangles) and after (open circles) the adsorption of the PSS layer ($N = 2520$, $f = 37\%$). In this representation, the presence of the PSS layer is clearly evidenced, the $q^4R$ curve being first below, crossing at $q \approx 1$ nm$^{-1}$ and staying finally above that of the bare surface. Therefore, the contribution of the PSS layer is qualitatively given by the difference $\Delta q^4R$ defined as follows :

$$\Delta q^4 R = q^4 R_{\text{after adsorption}} - q^4 R_{\text{before adsorption}} \qquad (5)$$

$\Delta q^4R$ is plotted in figure 5 as a function of $q$ for a series of PSS of a chain length $N = 930$ and various chemical charge fractions $f$. It shows a strong dependence of $\Delta q^4R$, *i. e.*, of the layer characteristics, on $f$. For the

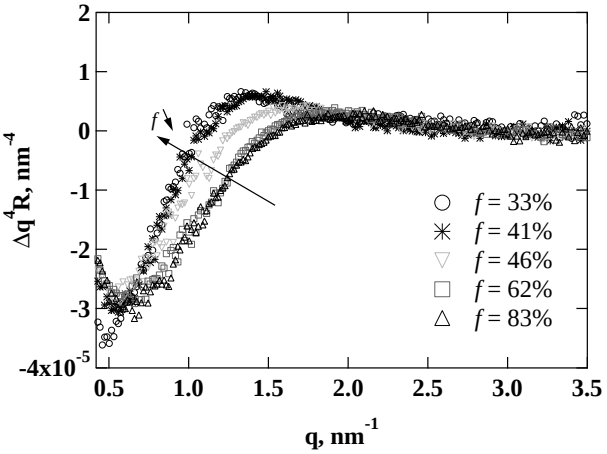


FIG. 5: $\Delta q^4R$ as a function of the vertical momentum transfer $q$ for PSS of chain length $N = 930$ and various chemical charge fractions $f$. The arrow indicates decreasing values of $f$

sake of comparison, the same experiment has been performed with the model hydrophilic polyelectrolyte called AMAMPS. In figure 6, $\Delta q^4R$ is plotted as a function of $q$ for AMAMPS of various chemical charge fractions in the same range as those in figure 5. Here the $\Delta q^4R$ curves are superposable, indicating that the properties of the adsorbed AMAMPS layer are independent of $f$ [26]. These experiments show a clear difference in the adsorption behavior of the hydrophilic polyelectrolytes and the

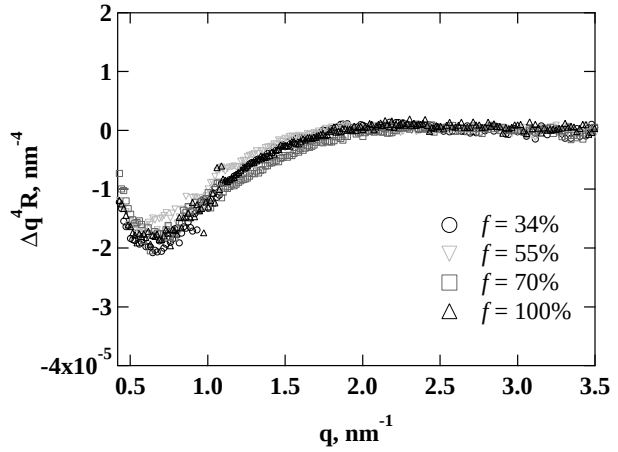


FIG. 6: $\Delta q^4 R$ as a function of the vertical momentum transfer $q$ for AMAMPS (hydrophilic polyelectrolyte) of various chemical charge fractions $f$.

hydrophobic ones. At this point, one should recall that the bulk solution properties of the same polymers are also markedly different. For AMAMPS, it has been shown that the structure of the solution is independent of $f$ in the range where the effective charge fraction is renormalized by Manning condensation to a constant value of 36% [1, 21]. In contrast, for PSS solutions, the structural characteristics all depend on $f$ and corroborate the pearl-necklace conformation of the single chain ([9] and references therein). At the same time the effective charge has been found to be a strong function of $f$ (see eq. 1). It is tempting to assume that the chain conformation at the surface is related to that in the bulk and that the evolution of the adsorbed PSS layer properties on $f$ observed in figure 5 are related to conformational effects, *i. e.*, the presence of pearls in the specific case of hydrophobic polyelectrolytes.

In what follows, we will focus on the evolution of the PSS layer thickness as a function of the effective charge fraction.

### B. Data analysis

Quantitative analysis have been performed by fitting the experimental reflectivity curves with the recursive Parratt algorithm [27]. Our system has been modeled as a stratified medium composed of layers numbered from 0 (water) to $n$ (silicon). In layer $j$, the propagating vector projection along the vertical direction is

$$k_j \approx \frac{2\pi}{\lambda}\sqrt{\theta^2 + 2(\delta_0 - \delta_j) + 2i(\beta_0 - \beta_j)} \qquad (6)$$

The amplitude of the reflection coefficient for the electric field $r_{j-1,j}$ at the interface separating layer $j-1$ and layer $j$ is given by

$$r_{j-1,j} = a_{j-1}^2 \frac{r_{j,j+1} + F_{j-1,j}}{r_{j,j+1}F_{j-1,j} + 1} \qquad (7)$$

where

$$a_{j-1} = \exp(-ik_j h_j) \qquad (8)$$

is the delay produced by the layer $j$ of thickness $h_j$ and $F_{j-1,j}$ the Fresnel coefficient given by

$$F_{j-1,j} = \frac{k_{j-1} - k_j}{k_{j-1} + k_j} \exp(-2k_{j-1}k_j\sigma_{j-1,j}^2) \qquad (9)$$

introducing the Nevot and Croce roughness $\sigma_{j-1,j}$ of the interface between layer $j-1$ and layer $j$ [28]. This recursive system is solved knowing $r_{n,n+1} = 0$ and the reflectivity is given by

$$R = |r_{0,1}r_{0,1}^*|^2 \qquad (10)$$

where $r_{0,1}^*$ is the complex conjugate of $r_{0,1}$. The quality of the fit of the experimental data is illustrated by the solid lines in figure 4. For all the data, the above algorithm has been performed using three fitting parameters : the PSS layer thickness $h_{PSS}$, its roughness $\sigma_{PSS}$ and its electron density $\rho_{PSS}$. For each substrate, all other parameters have been fixed ($\rho_{Si} = 0.70$ e$^-$Å$^{-3}$, $\sigma_{Si} = 0.5$ nm, $\rho_{SiO2} = 0.67$ e$^-$Å$^{-3}$, $\rho_{H2O} = 0.33$ e$^-$Å$^{-3}$) or measured independently by ellipsometry ($h_{Si02}$) and *in situ* high energy reflectivity prior to polyelectrolyte adsorption ($h_{SAM}$, $\rho_{SAM}$, $\sigma_{SAM}$). It is important to note that, whereas the thickness and roughness of the SAM inside water has been found to be the same as that measured in air (by ellipsometry and X-ray reflectivity), its electron density systematically shifted from 0.29 e$^-$Å$^{-3}$ in air to 0.45 e$^-$Å$^{-3}$ in pure water [29]. Only this later value allowed to fit the reflectivity profiles of the PSS layers and was used throughout.

### C. Electron density and roughness

The electron density $\rho_{PSS}$ was found to increase as a function of $f$ from 0.36 to 0.40 e$^-$Å$^{-3}$. This is to be expected since most of the contrast comes from the counterions in the layer. Indeed, according to the $f_{eff}$ values (listed in table I), the amount of condensed counter-ions per chain varies within a factor of 2 in the $f$ range explored. Assuming that the adsorbed amount remains constant as verified by *in situ* ellipsometry [18], the electron density should increase accordingly. On the other hand, the roughness of the PSS layer has been measured to be between 1.0 and 1.5 nm. To be meaningful, this value has to be compared to the thickness of the adsorbed layer, typically between 1 and 5 nm (see next subsection). There is thus a strong coupling between the roughness and the thickness and a precise determination of each

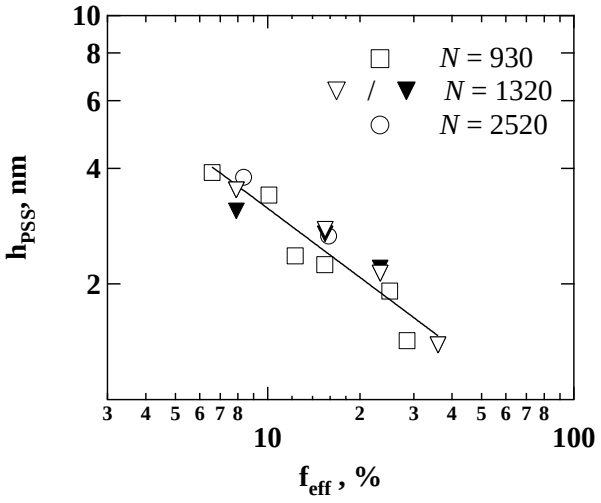


FIG. 7: Thickness $h_{PSS}$ of the adsorbed PSS layer as a function of the effective charge fraction $f_{eff}$ for various chain lengths $N$. The straight line has a slope of -2/3. The open symbols correspond to the adsorption onto oppositely charge surfaces, the filled inverted triangles to the adsorption onto hydrophobic surfaces. Errors on experimental points are around 0.4 nm.

parameter independently is difficult. Nevertheless, there is a clear evidence of the rough character of the adsorbed layer at a molecular level. This is qualitatively in agreement with the presence of pearls composing the adsorbed PSS layer.

### D. Thickness

In figure 7, the thickness $h_{PSS}$ of the PSS layers, is plotted as a function of the effective charge fraction $f_{eff}$. Let us first consider the adsorption of PSS onto oppositely charged surfaces (open symbols). $h_{PSS}$ decreases with $f_{eff}$ and is independent of $N$ at least for the large molecules considered here ($N \geq 930$) [30]. Since $\rho_{PSS}$ and $\sigma_{PSS}$ appear only slightly dependent on $f$, the strong evolution with $f$ observed in figure 5 is mostly due to variations of $h_{PSS}$. As shown in figure 7, $h_{PSS}$ and $f_{eff}$ span slightly less than a decade. It is thus impossible to determine whether a power law exists and what the precise value of the $f_{eff}$ exponent would be. Nevertheless, within experimental accuracy, the $h_{PSS}$ dependence on $f_{eff}$ is in agreement with the predicted power law:

$$h_{PSS} \propto aN^0 f_{eff}^{-2/3} \tag{11}$$

as represented by the straight line in figure 7. For all films, the thickness was the same in the adsorbing solution or after flushing with pure water, indicating that all adsorbed chains are strongly attached to the surface and do not desorb. On the other hand, the results of figure 7 and eq. 11 are in perfect agreements with previous results from *in situ* ellipsometry experiments performed on the same system [18]. In contrast to ellipsometry, X-ray reflectivity does not require any assumption on the refractive index and allows one to establish the electron density profile. X-ray reflectivity is thus a reliable and accurate technique to fully characterize a polyelectrolyte monolayer at a solid-liquid interface.

It is worth recalling that we have chosen the conditions of adsorption in order to estimate the pearl size. For this purpose, the adsorption has been made in the presence of added salts so that the Debye length is comparable to the pearl size. As it has been shown experimentally [18] and predicted theoretically [31], the pearl-necklace conformation persists upon adsorption in these conditions of screened electrostatic attraction to the surface. Furthermore, the electrostatic repulsion between two neighbouring pearls is sufficiently screened to induce a compaction of the pearl-necklace on its pearls [32]. Therefore, the PSS layer can be viewed as dense carpet of pearls. The thickness $h_{PSS}$ is closely related to the pearl size $D_p$ and we assume that $h_{PSS}$ is proportional $D_p$:

$$h_{PSS} \propto D_p \tag{12}$$

By analogy with the Rayleigh instability of a charged droplet [33], the pearl-size is predicted [5] to scale as:

$$D_p \propto aN^0 \lambda^{-2/3} \tag{13}$$

where $\lambda$ is the linear charge density along the chain. For a real polyelectrolyte system, we assume that $\lambda$ is given by the effective charge fraction $f_{eff}$ and we expect:

$$D_p \propto aN^0 f_{eff}^{-2/3} \tag{14}$$

Therefore, the experimental results of figure 7 and eq. 11 are in perfect agreement with the scaling predictions of the pearl-necklace model for the pearl size (eq. 14). This is an indirect experimental evidence of the pearl-necklace conformation induced by a Rayleigh-like instability. This confirms that the effective charge fraction $f_{eff}$, rather than $f$, is also controlling the intra-chain electrostatic interactions.

### E. Adsorption onto hydrophobic surfaces

All previous results concerned the adsorption on positively charged surfaces (PCS). We have to be concerned with the deformation of pearls upon adsorption since a strong flattening of pearls has also been predicted in the case of unscreened attraction [34]. For this purpose, we have also studied, in a less extended way, the adsorption of PSS onto hydrophobic surfaces (HS). This corresponds to the filled symbols in figure 7. Before all, it is important to note that the kinetics of adsorption differs largely from that of electrostatic adsorption [35]. In the former case, chains have to diffuse towards the HS and the adsorption process is slow whereas in the latter, the

adsorption to the PCS is driven by electrostatic attraction. In order to measure the equilibrium thickness in the case of HS, $h_{PSS}$ has been measured after a contact time of 24 hours between the surface and the PSS solution. Data of figure 7 are preliminary results and only three points have been obtained. Nevertheless, within experimental accuracy, it seems that the behaviour on HS surface is identical to that on PCS. In other words, the pearl-necklace conformation seems to persist also upon adsorption onto hydrophobic surfaces. We are now pursuing this study and we expect that further experiments will elucidate this interesting point.

## IV. CONCLUSION

The model hydrophobic polyelectrolyte poly(styrene-*co*-styrene sulfonate), called PSS, of various chain lengths $N$ and effective charge fractions $f_{eff}$ has been adsorbed onto oppositely charged surfaces immersed in water. An original technique, *in situ* high energy X-ray reflectivity, has allowed us to measure the electron density $\rho_{PSS}$, the roughness $\sigma_{PSS}$ and the thickness $h_{PSS}$ of the PSS monolayer at the buried solid-liquid interface. In the presence of an adequate amount of added salts, all measured parameters are a strong function of the charge fraction in marked contrast to the case of a hydrophilic (AMAMPS) adsorbed in the same conditions. We have found $h_{PSS} \propto aN^0 f_{eff}^{-2/3}$ in agreement with the scaling prediction for the pearl-size $D_p$ in the pearl-necklace model if one interprets $h_{app}$ as a measure of $D_p$. Preliminary investigations of PSS layers adsorbed on a hydrophobic solid surface at the same ionic strength point to a very similar structure of the layers. Further experiments will analyze the off-specular reflectivity in order to characterize the in-plane structure of the PSS layer.

### Acknowledgments

It is a pleasure to thank Jean Daillant for illuminating discussions about the intricacies of X-ray reflectivity and for his active help when first setting up the experiment. We also wish to thank Victor Etgens for sharing with us his ideas about the design of the cell. The efficient help of the technical and scientific staff of ESRF, particulary O. Konovalov, B. Jean and O. Plantevin, is gratefully acknowledge. C. Monteux kindly assisted us for one set of experimental runs.

[1] D. Baigl, Ph.D. thesis, Paris VI, Paris, France (2003), http://tel.ccsd.cnrs.fr/documents/archives0/00/00/36/20/tel-00003620-00/tel-00003620.pdf.
[2] M.-J. Lee, M. M. Green, F. Mikeš, and H. Morawetz, Macromolecules **35**, 4216 (2002).
[3] M. Rawiso, private communication, July 2003.
[4] Y. Kantor and M. Kardar, Europhys. Lett. **27**, 643 (1994).
[5] A. V. Dobrynin, M. Rubinstein, and S. P. Obukhov, Macromolecules **29**, 2974 (1996).
[6] A. V. Dobrynin and M. Rubinstein, Macromolecules **32**, 915 (1999).
[7] U. Micka, C. Holm, and K. Kremer, Langmuir **15**, 4033 (1999).
[8] H.-J. Limbach and C. Holm, J. Phys. Chem. B **107**, 8041 (2003).
[9] D. Baigl, R. Ober, D. Qu, A. Fery, and C. E. Williams, Europhys. Lett. **62**, 588 (2003).
[10] D. Qu, D. Baigl, C. E. Williams, H. Mohwald, and A. Fery, Macromolecules **36**, 6878 (2003).
[11] H.-J. Limbach, C. Holm, and K. Kremer, Europhys. Lett. **60**, 566 (2002).
[12] A. Kyriy, G. Gorodyska, S. Minko, W. Jaeger, P. Štěpànek, and M. Stamm, J. Am. Chem. Soc. **124**, 13454 (2002).
[13] B. V. Styrkas, D. A., J. R. Lu, J. L. Keddie, and S. P. Armes, Langmuir **16**, 5980 (2000).
[14] J. Daillant and A. Gibaud, eds., *X-ray and neutron reflectivity: principles and applications* (Springer, Berlin, 1999).
[15] A. Plech and T. Salditt, in *Handbook of polyelectrolytes and their applications* (Stevenson Ranch, CA, USA, 2002), vol. 1, p. 265.
[16] W. H. de Jeu, Rev. Mod. Phys. **75**, 181 (2003).
[17] A. Plech, T. Salditt, C. Münster, and J. Peisl, J. Colloid Interface Sci. **223**, 74 (2000).
[18] D. Baigl, M. Sferrazza, and C. E. Williams, Europhys. Lett. **62**, 110 (2003).
[19] O. Théodoly, R. Ober, and C. E. Williams, Eur. Phys. J. E. **5**, 51 (2001).
[20] D. Baigl, T. A. P. Seery, and C. E. Williams, Macromolecules **35**, 2318 (2002).
[21] W. Essafi, D. Baigl, and C. E. Williams, in preparation.
[22] C. L. McCormick and G. S. Chen, J. Polym. Sci.: Polym. Chem. Ed. **20**, 817 (1982).
[23] P. S. Pershan and J. Als-Nielsen, Phys. Rev. Lett. **52**, 759 (1984).
[24] If the same experiment had been made at 8 keV, the energy of the cupper K$\alpha_1$ radiation provided by a rotating anode, the absorption coefficient would have been $\alpha \approx 10^{-11}$.
[25] Preliminary measurements were also performed at a photon energy of 18 to 20 keV. See *ESRF highlights* 1997/1998, pp. 20-21.
[26] Corresponding to these curves, the fits have provided the following parameters for the adsorbed AMAMPS (hydrophilic polyelectrolyte) monolayer: $h_{AMAMPS} \approx 2$ nm, $\rho_{AMAMPS} \approx 0.35$ e$^-$Å$^{-3}$, $\sigma_{AMAMPS} \approx 1.0$ nm. These parameters are independent of $f$, as illustrated by figure 6.
[27] L. G. Parratt, Phys. Rev. **95**, 359 (1954).
[28] L. Nevot and P. Croce, Rev. Phys. Appl. **15**, 761 (1980).
[29] This anomalous increase was also observed in recent experiments on other interfaces in water [36, 37].

[30] In the case of sufficiently short chains, a globular state is expected and $h$ depends on $N$, as shown in [18].
[31] A. V. Dobrynin and M. Rubinstein, Macromolecules **35**, 2754 (2002).
[32] In solution, the pearl characteristics (conformation and size) are insensitive to the presence of added salt, as shown by Zero Average Contrast Neutron Scattering (ZAC SANS) experiments. M.-N. Spitteri, PhD thesis, Paris XI, Orsay, France (1997).
[33] J. W. S. Rayleigh, Phil. Mag. **14**, 184 (1882).
[34] O. V. Borisov, F. Hakem, T. A. Vilgis, J.-F. Joanny, and A. Johner, Eur. Phys. J. E. **6**, 37 (2001).
[35] O. Théodoly, Ph.D. thesis, Paris VI, Paris, France (1999).
[36] A. K. Doer, M. Tolan, J.-P. Schlomka, and W. Press, Europhys. Lett. **52**, 330 (2000).
[37] D. Schwended, T. Hayashi, R. Steitz, R. Dahint, J. Pipper, A. Pertsin, and M. Grunze, Langmuir **19**, 2284 (2003).